Title
Comparison of three empirical force fields for phonon calculations in CdSe quantum dots

Journal
The Journal of Chemical Physics, 144(21)

ISSN
0021-9606

Author
Kelley, Anne Myers

Publication Date
2016-06-07

DOI
10.1063/1.4952990

Peer reviewed

Comparison of three empirical force fields for phonon calculations in CdSe quantum dots

Anne Myers Kelley

Chemistry & Chemical Biology, University of California, Merced, 5200 North Lake Road, Merced, CA 95343

Abstract

Three empirical interatomic force fields are parametrized using structural, elastic, and phonon dispersion data for bulk CdSe and their predictions are then compared for the structures and phonons of CdSe quantum dots having average diameters of ~2.8 and ~5.2 nm (~410 and ~2630 atoms, respectively). The three force fields include one that contains only two-body interactions (Lennard-Jones plus Coulomb), a Tersoff-type force field that contains both two-body and three-body interactions but no Coulombic terms, and a Stillinger-Weber type force field that contains Coulombic interactions plus two-body and three-body terms. While all three force fields predict nearly identical peak frequencies for the strongly Raman-active "longitudinal optical" (LO) phonon in the quantum dots, the predictions for the width of the Raman peak, the peak frequency and width of the infrared absorption peak, and the degree of disorder in the structure are very different. The three force fields also give very different predictions for the variation in phonon frequency with radial position (core versus surface). The Stillinger-Weber plus Coulomb type force field gives the best overall agreement with available experimental data.

Introduction

The equilibrium geometry of a collection of atoms--small molecule, macromolecule, bulk crystal, or nanocrystal--can be defined as the set of atomic positions at which there are no net forces on any of the atoms and all second derivatives of the potential energy with respect to pairs of coordinates are positive. The harmonic vibrational frequencies and normal modes of vibration depend on the equilibrium positions and masses of the atoms and the second derivatives of the potential energy. Computational determination of these quantities requires knowledge of the potential energies through which the atoms interact—the interatomic force field. In principle, the force field is determined quantum mechanically by solving the Schrödinger equation for the total energy of the system as a function of nuclear position. In practice, computers and electronic structure methods for approximate solution of the Schrödinger equation are now fast enough to allow fairly accurate calculation of geometries and vibrational frequencies for small to medium sized molecules and very small nanocrystals, but it is still rarely practical to carry out such calculations for systems with thousands of atoms. Thus, empirically parameterized interatomic potentials are still widely employed for calculations of equilibrium geometries, dynamics, and vibrations of macromolecules and nanomaterials.

Empirical force fields have been developed for a number of single-component and binary semiconductors. These have been employed chiefly in molecular dynamics simulations of processes such as surface reconstruction and phase transitions,[1-19] but there has also been interest in using empirical potentials to calculate the geometries and vibrations of semiconductor nanocrystals ("quantum dots" when nearly spherical).[20-28] Our group has been using quantitative resonance Raman intensity analysis to probe electron-phonon coupling in

CdSe-containing quantum dots (QDs),[29-33] and full interpretation of these data requires knowledge of the phonon frequencies and modes. While the vibrational properties of molecules and nanomaterials are determined largely by the masses and connectivities of the atoms, the details can be quite dependent upon the specific force field used. Furthermore, different force fields that give about equally good agreement with experiment for bulk semiconductors may make very different predictions for the structures and phonon properties of nanocrystals.

This paper compares predictions for the geometries and vibrational properties of CdSe quantum dots using three different empirical force fields. The first is the potential originally developed by Rabani[34] and since employed for a wide variety of structural and dynamic calculations on both bulk and nanostructured CdSe.[8-12,16,17,35] The Rabani potential contains only two-body interactions: the Coulombic attractions and repulsions between pairs of ions, and a Lennard-Jones 6-12 attractive-repulsive interaction between each pair of ions. The second is a potential of the Tersoff type[36] that is more often used for single-component semiconductors. It contains both two-body (bond stretching and nonbonded) and three-body (bond angle bending) interaction terms. The third is a potential of the type developed by Han and Bester for III-V semiconductors,[20] which combines Coulombic terms with a Stillinger-Weber type, two-body plus three-body force field. In each case the parameters of the force field are first adjusted to reasonably well reproduce the lattice parameters, elastic constants, and phonon frequencies of bulk CdSe. These force fields are then used to calculate equilibrium geometries and a variety of vibrational properties for two sizes of CdSe quantum dots. Where possible, these predictions are compared with experimental observations.

Methods

The first interatomic potential employed was the Rabani two-body potential,[34] which consists of a Lennard-Jones term plus a Coulomb term:

$$V_{Rabani} = \sum_i \sum_{j>i} \frac{q_i q_j}{r_{ij}} + 4\epsilon_{ij}\left\{\left(\frac{\sigma_{ij}}{r_{ij}}\right)^{12} - \left(\frac{\sigma_{ij}}{r_{ij}}\right)^{6}\right\} \quad (1)$$

The Rabani potential was used with its original parameters,[34] which are listed in Table 1.

Table 1. Parameters of Rabani force field (eq. 1).

parameter	q	σ / Å	ϵ / meV
Cd	1.18	1.98	1.4477
Se	-1.18	5.24	1.2840

Combining rules: $\epsilon_{ij} = \sqrt{\epsilon_i \epsilon_j}$ and $\sigma_{ij} = \frac{1}{2}(\sigma_i + \sigma_j)$

The second was a potential described by Benkabou,[36] in which the interatomic interactions are of the Tersoff form. This potential contains no explicit Coulombic interactions but has both two-body and three-body terms:

$$V_{Tersoff} = \sum_i \sum_{j>i} f_c(r_{ij})\left[A exp(-\lambda_1 r_{ij}) - B b_{ij} exp(-\lambda_2 r_{ij})\right] \quad (2a)$$

where

$$f_c(r_{ij}) = \begin{cases} 1, & r < R - D \\ \frac{1}{2} - \frac{1}{2} sin\left[\frac{\pi}{2}\frac{(r-R)}{D}\right], & R - D < r < R + D \\ 0, & r > R + D \end{cases} \quad (2b)$$

and

$$b_{ij} = \left(1 + \beta^n \xi_{ij}^n\right)^{-1/(2n)} \quad (2c)$$

$$\xi_{ij} = \sum_{k \neq i,j} f_c(r_{ij}) g(\theta_{ijk}) \quad (2d)$$

$$g(\theta) = 1 + \frac{c^2}{d^2} - \frac{c^2}{d^2 + (h - cos\theta)^2} \quad (2e)$$

The parameters of the Tersoff potential were slightly adjusted from those originally reported by Benkabou[36] to better reproduce parameters of bulk CdSe.[33] The final parameters are listed in Table 2.

Table 2. Parameters of Tersoff potential (eqs. 2).

parameter	value
A / eV	5214
B / eV	239.5
λ_1 / Å^{-1}	3.1299
λ_2 / Å^{-1}	1.7322
β	1.5724 x 10^{-6}
n	0.78734
c	100390
d	16.217
h	-0.57058
R / Å	3.175
D / Å	0.15

The third potential tested was a modification of the force field developed by Han and Bester for III-V materials,[20] which combines the two-body and three-body terms of a Stillinger-Weber type potential with a Coulomb potential:

$$V = \sum_{i<j}^{1NN} V_2(i,j) + \sum_{i<k}^{2NN} V_2(i,k) + \sum_{i<j<k} V_3(i,j,k) + \sum_{i<j} V_C(i,j) \quad (3a)$$

where $1NN$ and $2NN$ refer to first and second nearest neighbor atoms,

$$V_2(i,j) = \begin{cases} A\left(\frac{B}{r_{ij}^4} - 1\right) exp\left(\frac{\rho}{r_{ij}-b}\right), & r_{ij} < b \\ 0, & r_{ij} > b \end{cases} \quad (3b)$$

$$V_3(i,j,k) = h(r_{ij}, r_{ik}) + h(r_{ji}, r_{jk}) + h(r_{ki}, r_{kj}) \quad (3c)$$

where

$$h(r_{ij}, r_{ik}) = \lambda exp\left(\frac{\eta}{r_{ij}-b} + \frac{\eta}{r_{ik}-b}\right)\left(cos\theta_{jik} + \frac{1}{3}\right)^2 \quad (3d)$$

and

$$V_C(i,j) = \frac{z_i z_j}{|r_{ij}|} \qquad (3e)$$

The parameters of the Bester potential were refined, starting from those obtained by Han and Bester for InAs,[20] to adequately reproduce bulk parameters of CdSe.[31] The final parameters employed are collected in Table 3.

Table 3. Parameters of Bester potential (eqs. 3).

parameter	value
|Z|	0.83
$A_{Cd\text{-}Cd}$ / eV	1.218
$A_{Cd\text{-}Se}$ / eV	1.885
$A_{Se\text{-}Se}$ / eV	1.806
$B_{Cd\text{-}Cd}$ / Å^4	208.9
$B_{Cd\text{-}Se}$ / Å^4	87.01
$B_{Se\text{-}Se}$ / Å^4	20.04
b_{1NN} / Å	4.1074
b_{2NN} / Å	5.64
ρ / Å	2.28
λ / eV	27.9402
θ / degrees	109.47
η / Å	2.8697

Calculations on nanocrystals were carried out using the general methods described in our earlier publications.[31-33,37] Briefly, a bulk wurtzite CdSe lattice was generated, an origin and a radius were chosen, and all atoms beyond that radius were eliminated, as were any remaining surface atoms having fewer than two nearest neighbors. The General Utility Lattice Program (GULP 4.0)[38] was then used to find the equilibrium geometry and the harmonic vibrational frequencies and normal modes with each of the three empirical force fields. Calculations were performed on four "small" quantum dots (diameter ~2.8 nm, 405-413 atoms) and four "large"

quantum dots (diameter ~5.2 nm, 2633-2640 atoms), with the different structures obtained by choosing different locations for the origin relative to the center of the unit cell. Some of these structures were stoichiometric while others had small excesses (five atoms or fewer) of either ion. None of the minimized structures had any imaginary vibrational frequencies larger than 1 cm^{-1}, meaning that they were very close to a true energy minimum.

Calculations of the structures, elastic constants, and phonon dispersion curves of bulk CdSe were also carried out using the GULP program.

Raman intensities on resonance with the lowest excitonic transition ($1S_e1S_h$) were calculated as described previously.[31,32] Briefly, the electron and hole wavefunctions were calculated using the effective mass approximation particle in a sphere model and the electric field produced by the resulting electron and hole charge distributions was used to calculate the electron-phonon coupling for each vibrational mode via the Fröhlich mechanism. For these comparisons, S-D mixing in the valence band was not included and the electron-hole interaction was not considered in calculating the excitonic wavefunctions. The Raman spectra were calculated by assuming that the Raman intensity of each normal mode is proportional to its frequency squared multiplied by its Huang-Rhys factor,[37] and assigning each transition a Lorentzian envelope with a width of 5 cm^{-1}. The infrared spectra were calculated by assigning each normal mode an intensity proportional to the square of the dipole moment induced by the vibration, with each transition having the same Lorentzian lineshape used for the Raman calculations. (Although the Tersoff potential assumes no charges on the atoms, charges equal to those for the Bester potential were assumed for the purpose of calculating the Raman and infrared intensities.)

The average radial position of each mode and the radial versus transverse character of each mode were calculated from the phonon eigenvectors as described in ref. 33. Specifically, the radial position is defined as

$$R_i = \frac{1}{r_{avg}} \frac{\sum_j |\vec{v}_{j,i}| r(j)}{\sum_j |\vec{v}_{j,i}|} \quad (4)$$

where the sums are over all atoms, $r(j)$ is the radial distance of atom j from the origin, $\vec{v}_{j,i}$ is the displacement of atom j in mode i, and $r_{avg} = \frac{\sum_j r(j)}{N_{atom}}$ is the average radial distance from the origin. With this definition, R_i = 1 if the displacements are, on average, distributed equally among atoms independent of their distance from the origin, a surface localized mode has $R_i > 1$, and a mode localized to the interior of the QD has $R_i < 1$. The radial character of the mode is defined by

$$C_i = \sum_j \left| \hat{v}_{j,i} \cdot \hat{r}_j \right| \left(\frac{|\vec{v}_{j,i}|}{\sum_j |\vec{v}_{j,i}|} \right) \quad (5)$$

where $\hat{v}_{j,i}$ is the unit vector along the direction of the displacement of atom j in mode i and $\hat{r}_j$ is the unit vector along the radius of atom j. With this definition, $C_i = 0$ for purely tangential motion and $C_i = 1$ for purely radial motion. The extent of localization of each normal mode was described using the participation ratio defined as in ref. 39. The participation ratio of mode i is given by

$$p_i = \frac{\left(\sum_j |\vec{v}_{j,i}|^2 \right)^2}{N_{anion} \sum_j |\vec{v}_{j,i}|^4} \quad (6)$$

where the sums run over all of the anions and N_{anion} is the number of anions in the structure. In the limiting cases, if only one atom is moving, $p_i = \frac{1}{N_{anion}}$; if all of the atoms are moving the same amount, $p_i = 1$.

Results

Table 4 compares the experimental and calculated lattice parameters, elastic constants, and phonon frequencies at the gamma point for bulk wurtzite CdSe. Fig. 1 plots the experimental and calculated phonon dispersion curves from (0, 0, 0) to (0, 0, 0.5). The Bester potential gives the best fit to the experimental lattice constants, while the elastic constants are best reproduced by the Tersoff potential. The Rabani potential best fits the experimental dispersion curves for the lower-frequency phonons, while the Bester potential better reproduces the high-frequency optical phonon region. Overall, all three empirical potentials do a reasonably good job of reproducing the properties of the bulk crystal, and it is not immediately apparent that one potential is better than the others.

Table 4. Experimental and calculated lattice parameters, elastic constants, and phonon frequencies at Γ for bulk wurtzite CdSe.

	expt	Rabani	Tersoff	Bester
a / Å	4.30	4.38	4.35	4.31
c / Å	7.01	6.96	7.10	6.98
C_{11} / GPa	74.6	65.9	69.3	94.9
C_{12} / GPa	46.1	38.0	39.8	40.3
C_{13} / GPa	39.4	32.9	34.5	36.5
C_{33} / GPa	81.7	64.4	74.7	98.2
C_{44} / GPa	13.0	15.2	13.0	25.7
C_{66} / GPa	14.3	14.0	14.7	27.3
B / GPa	53.4	44.8	47.9	57.2
Γ freq* / cm^{-1}	33	51	47	65
Γ freq / cm^{-1}	116	131	130	163
Γ freq* / cm^{-1}	164	141, 151	183, 209	172, 174
Γ freq* / cm^{-1}	172	153	209, 213	175, 178
Γ freq / cm^{-1}	184	191	213	178
Γ freq / cm^{-1}	207	219	213	209

Lattice parameters, elastic constants C_{ij}, and bulk modulus B are from ref. 34. Phonon frequencies are from ref. 40. *Doubly degenerate frequency.

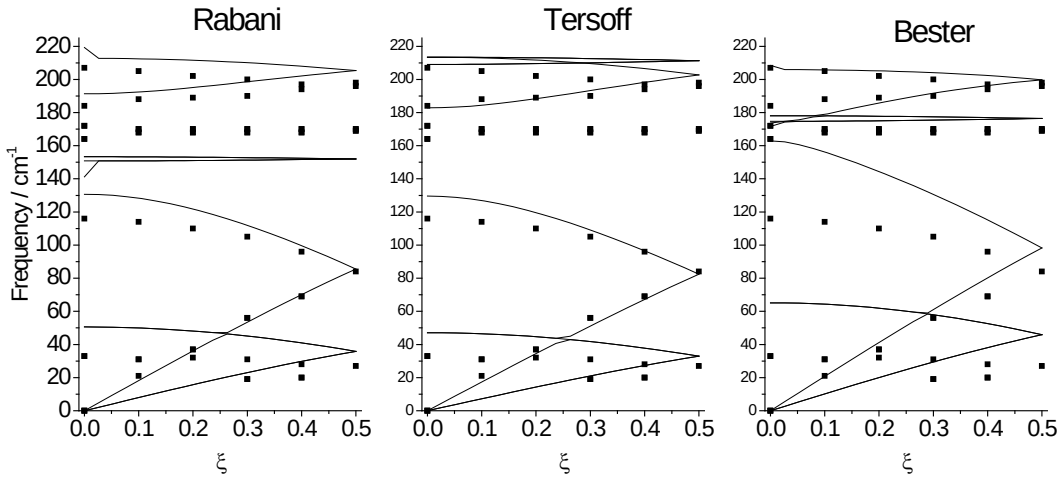

Figure 1. Experimental (points) and calculated (lines) phonon dispersion curves along (0, 0, 0) to (0, 0, 0.5). Experimental data are from ref. 40.

We now turn to the calculated properties of the quantum dots. In a previous publication[33] we noted that the Rabani potential predicts considerably disordered structures for nanocrystals while the Tersoff potential yields nanostructures that remain largely crystalline, in better agreement with experiment. Figures 2 and 3 show, for one small QD and one large QD from each potential, a histogram of the number of atoms at each z position, a crude proxy for the degree of crystallinity of each structure. Although none of the small QDs have perfectly ordered planes of atoms, the Tersoff structure appears to be the most crystalline and the Rabani structure the least. For the large QDs, the Bester potential gives by far the greatest degree of order as judged by the presence of well defined planes of atoms. While there was considerable variability among the eight different QDs examined, in all cases the structures calculated with the Rabani potential have far more disorder than with the other two potentials. This makes sense because the Rabani potential has no explicit angle-bending terms to maintain the tetrahedral ordering of the atoms when there are fewer than four nearest neighbors.

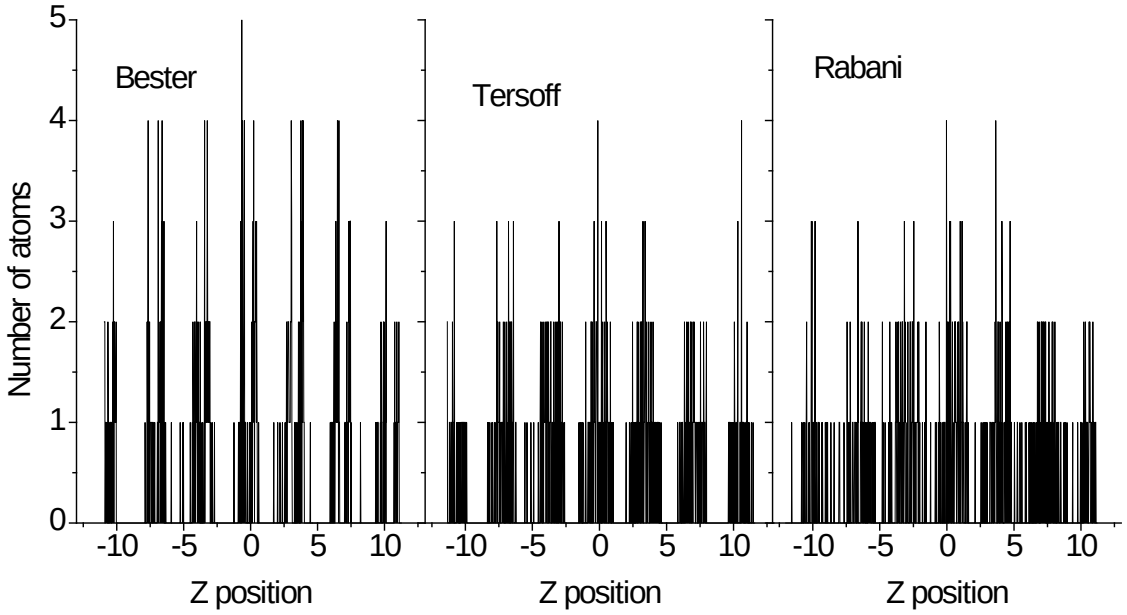

Figure 2. Positions of the atoms along the z axis for equilibrium geometries of the same original QD ($Cd_{206}Se_{206}$) calculated with three different interatomic potentials.

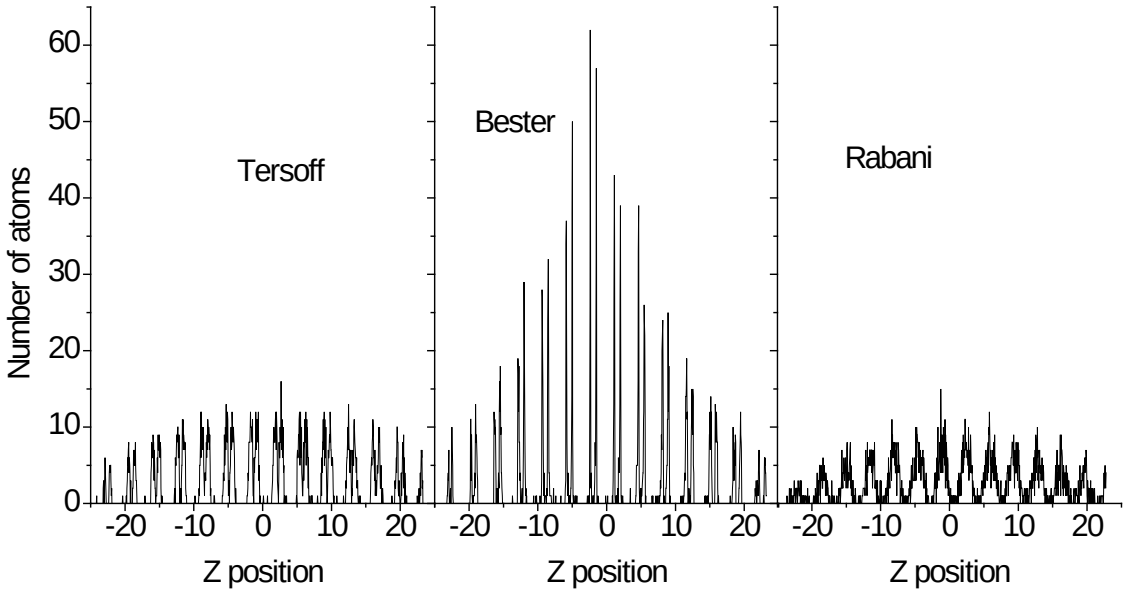

Figure 3. Same as Figure 2 for a larger QD ($Cd_{1321}Se_{1318}$).

Figure 4 compares a number of observable and unobservable properties of the phonons of the smaller QDs as calculated from the three potentials. Data from all four structures are averaged (for the spectra) or overlaid (for the other properties) to allow some consideration of

structural variation among QDs with essentially the same number of atoms. The upper plots show the calculated 1S-1S resonance Raman spectra and the IR spectra. The LO phonon peak in the Raman spectrum appears at 204-205 cm^{-1} in all three, but the acoustic phonons are relatively much more intense with the Tersoff potential and the Raman peak is much broader with the Rabani potential. All three potentials predict IR absorption spectra that are much broader than the resonance Raman spectra, but the Tersoff potential gives a peak in the IR spectrum at a slightly higher frequency than in the Raman spectrum while the Bester potential gives an IR peak at a frequency below that of the Raman. The Rabani potential calculates a very broad IR peak with its maximum at a much lower frequency.

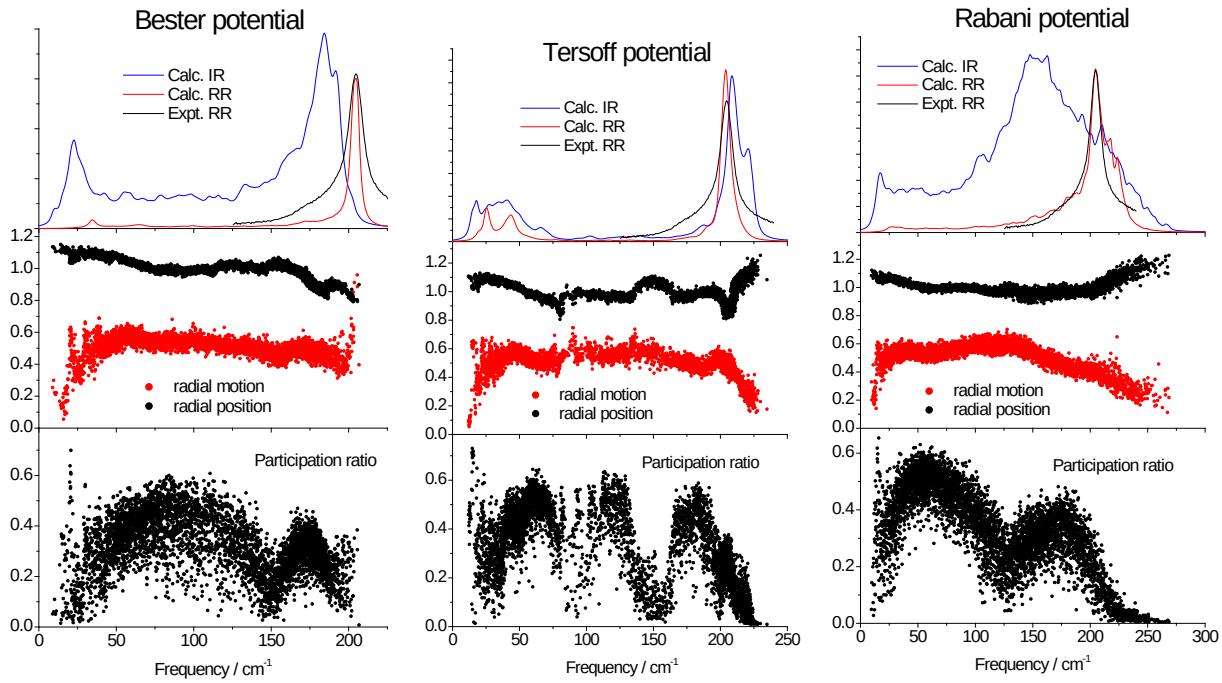

Figure 4. Top: calculated 1S-1S resonant Raman spectra (red) and infrared absorption spectra (blue) for 2.8 nm CdSe QDs calculated with the three different interatomic potentials. Also shown in black is the experimental resonance Raman spectrum of 3.1 nm CdSe QDs from ref. 31, plotted only from 105-245 cm^{-1} to avoid interference from Rayleigh and solvent scattering. Middle: Radial extent of the normal mode (black) and radial versus tangential character of the mode (red). Bottom: Participation ratio for each mode.

The middle plots in Fig. 4 show the average radial position of the moving atoms in each mode (a mode in which all atoms move the same amount would have a value of 1.0) and the radial versus tangential component of the motion (completely tangential or completely radial motion have values of 0 and 1, respectively). Focusing on the optical modes above ~170 cm^{-1}, for the Bester potential the higher-frequency modes tend to be slightly more localized in the core and the very highest-frequency modes are largely radial in character. For the Tersoff potential the more surface-localized modes have the highest frequency and are mostly tangential in character. The same is true of the Rabani potential but to a lesser degree.

Finally, the bottom plot in Fig. 4 shows the participation ratio, a measure of the extent of localization of the normal mode; it has a value of unity if all anions move the same amount in the normal mode, while in the opposite limit where only a single atom moves it has the value $1/N_{anion}$. For all three potentials there is a large spread in the participation ratios for different modes. In particular, the high-frequency, surface-localized modes calculated by the Tersoff and Rabani potentials involve relatively few atoms. It should be emphasized that the middle and lower panels of Fig. 4 show all of the phonons, while only a small fraction of those modes contribute significantly to either the Raman or the IR spectra.

Figure 5 shows the corresponding plots for the larger QDs (~5.2 nm diameter). Qualitatively, all of the trends observed for the smaller structures are also observed for the larger ones. The Raman peak frequencies increase with increasing size for all three potentials, although the shift for the Bester potential (1 cm^{-1}) is much smaller than for the Tersoff and Rabani potentials (6 cm^{-1} and 5 cm^{-1}, respectively); we observe an experimental shift of about 4 cm^{-1} over this size range. The Raman peaks are somewhat narrower in the larger QDs and the

separation between the Raman and IR peaks is somewhat less for all three potentials than in the smaller QDs. The general features of mode character versus frequency are similar for the small and large QDs, although the large QDs calculated with the Tersoff potential show a stronger partitioning into modes that are highly delocalized and those that are highly localized.

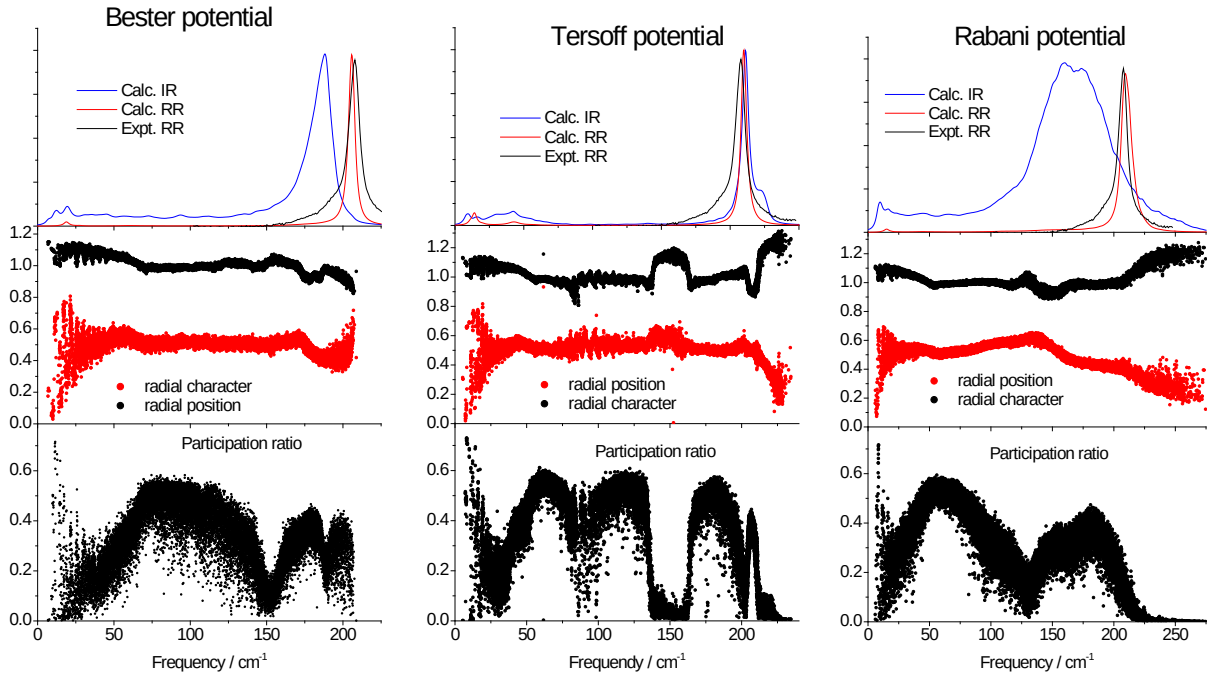

Figure 5. Same as Figure 4, for 5.2 nm CdSe QDs. The experimental resonance Raman spectrum is for 5.2 nm QDs from ref. 31.

Discussion

One approach to describing the vibrations of a nanocrystal is to assume that the nanocrystal is identical to the infinite bulk crystal apart from the boundary conditions. With this assumption, the each phonon of the nanocrystal is described as a linear combination of phonons of the bulk crystal having different wavevectors (the "phonon confinement" model).[41,42] This model predicts that the phonons of a quantum dot should be delocalized throughout the

structure, with different nodal patterns. In reality, however, the partial loss of crystalline order at the surfaces of the nanocrystal will break the degeneracy of the unit cells and should tend to localize the vibrational modes to some degree. A proper description of the true phonon eigenvectors is needed to fully interpret the excitation frequency-dependent resonance Raman spectra in terms of the spatial distribution of the various excitonic states and the magnitude of electron-phonon coupling. The extent to which the phonons are localized should also have implications for thermal transport and for exciton self-trapping (polaron formation) and subsequent hopping. As shown in Figures 2-5, the extent of this symmetry breaking-induced localization is predicted to be quite different in calculations carried out with different force fields. We do not know of any experimental measurements that directly probe the extent of phonon localization in CdSe QDs. However, the three force fields also make quite different predictions for the Raman and IR spectra and these can be compared with experimental data. CdSe QDs in the size range from 2.8-5.2 nm, when excited near the lowest excitonic absorption,[29,31-33] show a single well defined Raman peak in the LO phonon region with a frequency of 203-207 cm^{-1} and a full width at half maximum that does not exceed about 20 cm^{-1} including the effects of instrumental broadening and the distribution of sizes and shapes found in real samples. All three potentials give Raman spectra in reasonably good agreement with experiment for the larger QDs (Fig. 5 top), but for the smaller QDs the Rabani potential predicts a Raman spectrum that is already broader than the experiment (Fig. 4 top) even without any of the additional sources of experimental broadening. In addition, the prediction of the Tersoff model that the infrared absorption band has its maximum at a higher frequency than the Raman band is also inconsistent with experiment.[43,44] Few far-IR spectra of high quality CdSe QDs have

been reported, but the spectra of Ref. 44 on ~3.2 nm QDs (absorption maximum 550 nm) show a single, symmetric peak with its maximum at ~194 cm^{-1}, about 12 cm^{-1} lower than the Raman peak. When both the Raman and the IR spectra are considered, the Bester potential is the only one of the three force fields that produces QD vibrational spectra in reasonable agreement with experiment. It is perhaps relevant that the general form of this potential was developed with the explicit aim of correctly predicting phonon properties of large polar semiconductor nanostructures.[20]

The most obvious shortcoming of the general treatment described here is that it does not account for the ligands that usually cap the surface of quantum dots. Different synthetic methods produce QDs with a variety of "native" ligands, which are often deliberately exchanged with other ligands to provide desired stability, solubility, charge trapping, and/or reactivity.[45] We have not included surface ligands in these calculations because of the large number of different ligands that are used with CdSe and because of the additional ambiguities associated with determining appropriate force field parameters for the Cd- (or Se)-ligand interactions. Resonance Raman spectra generally show only a very weak dependence on surface ligands,[33] although some of the other phonon properties calculated here may be more sensitive. The vibrations of the ligands, including the Cd- or Se-ligand stretches, are normally not observed in resonance Raman spectra, indicating minimal delocalization of the charge carriers into the ligand shell. FTIR spectra clearly show the vibrations of the ligands,[46-48] but we are unaware of any direct IR observation of CdSe-ligand intermolecular modes. While inclusion of ligands may have some effect on the properties calculated here, the qualitative conclusions drawn from comparison of the force fields are unlikely to change.

The present treatment also ignores vibrational anharmonicities and calculates the vibrational properties at zero temperature. The measured anharmonicity of the LO phonon mode in CdSe nanocrystals is very small as estimated from overtone frequencies,[32] although the temperature dependence of the LO phonon frequency at higher temperatures suggests that anharmonic coupling to lower-frequency phonons is not negligible.[49,50] Again, while finite-temperature effects may modify the quantitative results obtained here, it is likely that the qualitative behavior of the force fields is adequately captured by the zero-temperature calculations.

The usual reason for carrying out phonon calculations such as these is to aid in the interpretation of experimental results. We give two examples. First, we measured resonance Raman spectra and cross-sections of CdSe QDs as a function of excitation wavelength and observed that the low-frequency shoulder on the LO phonon gains relative intensity as the excitation is tuned to higher energies.[33] This result implies that the main LO band and the low-frequency shoulder involve different atomic motions. The low-frequency shoulder had previously been assigned as a "surface optical" phonon based on dielectric continuum theory calculations of the phonons. Calculations on model structures using the Tersoff potential led us to conclude instead that the low-frequency shoulder involves LO-type modes that have more nodes in the vibrational wavefunction but are not significantly surface-localized.[33] Although the present calculations do not lead us to revise that conclusion, the qualitatively different results for some phonon properties obtained from different potentials reduce our confidence in their interpretive utility. Second, calculations on CdSe/CdS core/shell QDs using the Bester-type potential predict that the higher-frequency components of the CdS LO phonon involve more

motion of the atoms closest to the interface with the CdSe core, while the lower-frequency components involve more motion of surface atoms. This is contrary to the conclusions drawn from the measured excitation frequency dependence of the CdS LO phonon band shape and also from the expectation that mixing between the CdS modes and the lower-frequency CdSe modes should result in a frequency somewhat lower than that of a pure CdS structure.[32] The force field for core/shell structures requires, at a minimum, cross terms between Se and S at the interface, and there is no simple way to parameterize such a force field.

Recently Han and Bester carried out large-scale density functional theory calculations of core/shell quantum dots, including CdSe/CdS core/shell structures having up to 633 heavy atoms.[51] While these are still smaller than the structures on which most experiments are performed, they are large enough to be relevant to experimental systems. These calculations properly reproduce several features of the experimental resonance Raman spectra[32] including the shift to higher frequency of the CdSe core optical modes due to compression by the shell and the distribution of the CdS shell optical modes over a wide range of frequencies. They did not explicitly compare their results for either single-component or core/shell structures with any empirical force field results, noting the difficulty of incorporating the complex surface and interface effects. Indeed, inclusion of different force field parameters and Coulombic charges for surface and interface atoms will likely be necessary in order to achieve semiquantitative agreement with experiment. Approaches based on using a high quality density functional theory calculation to parameterize an empirical force field with a large number of parameters appear very promising.[52]

Acknowledgments

This work was supported by NSF grant #CHE-1506803.

References

(1) Grunwald, M.; Zayak, A.; Neaton, J. B.; Geissler, P. L.; Rabani, E. Transferable Pair Potentials for CdS and ZnS Crystals. *J. Chem. Phys.* **2012,** *136*, 234111.

(2) Henager, C., Jr.; Morris, J. R. Atomistic simulation of CdTe solid-liquid coexistence equilibria. *Phys. Rev.* **2009,** *80*, 245309.

(3) Tainter, C. J.; Schatz, G. C. Reactive Force Field Modeling of Zinc Oxide Nanoparticle Formation. *J. Phys. Chem. C* **2016,** *120*, 2950-2961.

(4) Wang, Z. Q.; Stroud, D.; Markworth, A. J. Monte Carlo study of the liquid CdTe surface. *Phys. Rev. B* **1989,** *40*, 3129-3132.

(5) Ward, D. K.; Zhou, X. W.; Wong, B. M.; Doty, F. P.; Zimmerman, J. A. Accuracy of existing atomic potentials for the CdTe semiconductor compound. *J. Chem. Phys.* **2011,** *134*, 244703.

(6) Zhou, X.; Ward, D. K.; Wong, B. M.; Doty, F. P.; Zimmerman, J. A. Molecular Dynamics Studies of Dislocations in CdTe Crystals from a New Bond Order Potential. *J. Phys. Chem. C* **2012,** *116*, 17563-17571.

(7) Zhou, X. W.; Ward, D. K.; Martin, J. E.; van Swol, F. B.; Cruz-Campa, J. L.; Zubia, D. Stillinger-Weber potential for the II-VI elements Zn-Cd-Hg-S-Se-Te. *Phys. Rev. B* **2013,** *88*, 085309.

(8) Grunwald, M.; Dellago, C. Transition state analysis of solid-solid transformations in nanocrystals. *J. Chem. Phys.* **2009,** *131*, 164116.

(9) Grunwald, M.; Rabani, E.; Dellago, C. Mechanisms of the wurtzite to rocksalt transformation in CdSe nanocrystals. *Phys. Rev. Lett.* **2006,** *96*, 255701.

(10) Ye, X.; Sun, D. Y.; Gong, X. G. Pressure-induced structural transformation of CdSe nanocrystals studied with molecular dynamics. *Phys. Rev. B* **2008,** *77*, 094108.

(11) Leoni, S.; Ramlau, R.; Meier, K.; Schmidt, M.; Schwarz, U. Nanodomain fragmentation and local rearrangements in CdSe under pressure. *Proc. Nat. Acad. Sci. USA* **2008,** *105*, 19612-19616.

(12) Zanjani, M. B.; Lukes, J. R. Size dependent elastic moduli of CdSe nanocrystal superlattices predicted from atomistic and coarse grained models. *J. Chem. Phys.* **2013,** *139*, 144702.

(13) Morgan, B. J.; Madden, P. A. Simulation of the pressure-driven wurtzite to rock salt phase transition in nanocrystals. *Phys. Chem. Chem. Phys.* **2006,** *8*, 3304-3313.

(14) Morgan, B. J.; Madden, P. A. A molecular dynamics study of structural relaxation in tetrahedrally coordinated nanocrystals. *Phys. Chem. Chem. Phys.* **2007,** *9*, 2355-2361.

(15) Wilson, M.; Hutchinson, F.; Madden, P. A. Simulation of pressure-driven phase transitions from tetrahedral crystal structures. *Phys. Rev. B* **2002,** *65*, 094109.

(16) Reed, E. J. Atomic transformation pathways from terahertz radiation generated by shock-induced phase transformations. *Phys. Rev. B* **2010,** *81*, 144123.

(17) Fan, Z.; Yalcin, A. O.; Tichelaar, F. D.; Zandbergen, H. W.; Talgorn, E.; Houtepen, A. J.; Vlugt, T. J. H.; van Huis , M. A. From Sphere to Multipod: Thermally Induced Transitions of

CdSe Nanocrystals Studied by Molecular Dynamics Simulations. *J. Am. Chem. Soc.* **2013,** *135*, 5869-5876.

(18) Fan, Z.; Koster, R. S.; Wang, S.; Fang, C.; Yalcin, A. O.; Tichelaar, F. D.; Zandbergen, H. W.; van Huis, M. A., *et al.* A transferable force field for CdS-CdSe-PbS-PbSe solid systems. *J. Chem. Phys.* **2014,** *141*, 244503.

(19) Wang, S.; Fan, Z.; Koster, R. S.; Fang, C.; van Huis, M. A.; Yalcin, A. O.; Tichelaar, F. D.; Zandbergen, H. W., *et al.* New Ab Initio Based Pair Potential for Accurate Simulation of Phase Transitions in ZnO. *J. Phys. Chem. C* **2014,** *118*, 11050-11061.

(20) Han, P.; Bester, G. Interatomic Potentials for the Vibrational Properties of III-V Semiconductor Nanostructures. *Phys. Rev. B* **2011,** *83*, 174304.

(21) Cheng, W.; Ren, S.-F. Calculations on the size effects of Raman intensities of silicon quantum dots. *Phys. Rev. B* **2002,** *65*, 205305.

(22) Ren, S.-F.; Cheng, W.; Yu, P. Y. Microscopic investigation of phonon modes in SiGe alloy nanocrystals. *Phys. Rev. B* **2004,** *69*, 235327.

(23) Cheng, W.; Ren, S.-F.; Yu, P. Y. Theoretical investigation of the surface vibrational modes in germanium nanocrystals. *Phys. Rev. B* **2003,** *68*, 193309.

(24) Fu, H.; Ozolins, V.; Zunger, A. Phonons in GaP quantum dots. *Phys. Rev. B* **1999,** *59*, 2881-2887.

(25) Ren, S.-F.; Lu, D.; Qin, G. Phonon modes in InAs quantum dots. *Phys. Rev. B* **2001,** *63*, 195315.

(26) Barrett, C.; Wang, L.-W. Double-charge model for classical force-field simulations. *Phys. Rev. B* **2015,** *91*, 235407.

(27) Qin, G.; Ren, S.-F. Effects of core size and shell thickness on phonon modes in GaAs/AlAs shell quantum dots. *J. Appl. Phys.* **2001,** *89*, 6037-6043.

(28) Han, P.; Bester, G. Confinement Effects on the Vibrational Properties of III-V and II-VI Nanoclusters. *Phys. Rev. B* **2012,** *85*, 041306(R).

(29) Baker, J. A.; Kelley, D. F.; Kelley, A. M. Resonance Raman and Photoluminescence Excitation Profiles and Excited-State Dynamics in CdSe Nanocrystals. *J. Chem. Phys.* **2013,** *139*, 024702.

(30) Kelley, A. M.; Dai, Q.; Jiang, Z.-j.; Baker, J. A.; Kelley, D. F. Resonance Raman Spectra of Wurtzite and Zincblende CdSe Nanocrystals. *Chem. Phys.* **2013,** *422*, 272-276.

(31) Lin, C.; Gong, K.; Kelley, D. F.; Kelley, A. M. Size Dependent Exciton-Phonon Coupling in CdSe Nanocrystals Through Resonance Raman Excitation Profile Analysis. *J. Phys. Chem. C* **2015,** *119*, 7491-7498.

(32) Lin, C.; Gong, K.; Kelley, D. F.; Kelley, A. M. Electron-phonon coupling in CdSe/CdS core-shell quantum dots. *ACS Nano* **2015,** *9*, 8131-8141.

(33) Lin, C.; Kelley, D. F.; Rico, M.; Kelley, A. M. The "Surface Optical" Phonon in CdSe Nanocrystals. *ACS Nano* **2014,** *8*, 3928-3938.

(34) Rabani, E. An Interatomic Pair Potential for Cadmium Selenide. *J. Chem. Phys.* **2002,** *116*, 258-262.

(35) Schapotschnikow, P.; Hommersom, B.; Vlugt, T. J. H. Adsorption and Binding of Ligands to CdSe Nanocrystals. *J. Phys. Chem. C* **2009,** *113*, 12690-12698.

(36) Benkabou, F.; Aourag, H.; Certier, M. Atomistic Study of Zinc-Blende CdS, CdSe, ZnS, and ZnSe from Molecular Dynamics. *Mat. Chem. Phys.* **2000,** *66*, 10-16.

(37) Kelley, A. M. Electron-Phonon Coupling in CdSe Nanocrystals from an Atomistic Phonon Model. *ACS Nano* **2011,** *5*, 5254-5262.

(38) Gale, J. D.; Rohl, A. L. The General Utility Lattice Program (GULP). *Molecular Simulation* **2003,** *29*, 291-341.

(39) Bell, R. J.; Dean, P.; Hibbins-Butler, D. C. Localization of normal modes in vitreous silica, germania and beryllium fluoride. *J. Phys. C* **1970,** *3*, 2111-2118.

(40) Widulle, F.; Kramp, S.; Pyka, N. M.; Gobel, A.; Ruf, T.; Debernardi, A.; Lauck, R.; Cardona, M. The Phonon Dispersion of Wurtzite CdSe. *Physica B* **1999,** *263-264*, 448-451.

(41) Silva, A. C. A.; Freitas Neto, E. S.; da Silva, S. W.; Morais, P. C.; Dantas, N. O. Modified Phonon Confinement Model and Its Application to CdSe/CdS Core-Shell Magic-Sized Quantum Dots Synthesized in Aqueous Solution by a New Route. *J. Phys. Chem. C* **2013,** *117*, 1904-1914.

(42) Richter, H.; Wang, Z. P.; Ley, L. The One Phonon Raman Spectrum in Microcrystalline Silicon. *Solid State Commun.* **1981,** *39*, 625-629.

(43) Vasiliev, R. B.; Vinogradov, V. S.; Dorofeev, S. G.; Kozyrev, S. P.; Kucherenko, I. V.; Novikova, N. N. IR-active vibrational modes of CdTe, CdSe, and CdTe/CdSe colloidal quantum dot ensembles. *J. Phys. Conf. Ser.* **2007,** *92*, 012054.

(44) Dzhagan, V. M.; Valakh, M. Y.; Milekhin, A. G.; Yeryukov, N. A.; Zahn, D. R. T.; Cassette, E.; Pons, T.; Dubertret, B. Raman- and IR-Active Phonons in CdSe/CdS Core/Shell Nanocrystals in the Presence of Interface Alloying and Strain. *J. Phys. Chem. C* **2013,** *117*, 18225-18233.

(45) Green, M. The nature of quantum dot capping ligands. *J. Mater. Chem.* **2010,** *20*, 5797–5809.

(46) Young, A. G.; Al-Salim, N.; Green, D. P.; McQuillan, A. J. Attenuated Total Reflection Infrared Studies of Oleate and Trioctylphosphine Oxide Ligand Adsorption and Exchange Reactions on CdS Quantum Dot Films. *Langmuir* **2008,** *24*, 3841-3829.

(47) Tan, Y.; Jin, S.; Hamers, R. J. Photostability of CdSe Quantum Dots Functionalized with Aromatic Dithiocarbamate Ligands. *ACS Appl. Mater. Inter.* **2013,** *5*, 12975−12983.

(48) von Holt, B.; Kudera, S.; Weiss, A.; Schrader, T. E.; Manna, L.; Parake, W. J.; Braun, M. Ligand exchange of CdSe nanocrystals probed by optical spectroscopy in the visible and mid-IR. *J. Mater. Chem.* **2008,** *18*, 2728-2732.

(49) Kusch, P.; Lange, H.; Artemyev, M.; Thomsen, C. Size-dependence of the anharmonicities in the vibrational potential of colloidal CdSe nanocrystals. *Solid State Commun.* **2011,** *151*, 67-70.

(50) Chen, L.; Rickey, K.; Zhao, Q.; Robinson, C.; Ruan, X. Effects of nanocrystal shape and size on the temperature sensitivity in Raman thermometry. *Appl. Phys. Lett.* **2013,** *103*, 083107.

(51) Han, P.; Bester, G. Heavy strain conditions in colloidal core-shell quantum dots and their consequences on the vibrational properties from *ab initio* calculations. *Phys. Rev. B* **2015,** *92*, 125438.

(52) Barrett, C.; Wang, L.-W. A systematic fitting procedure for accurate force field models to reproduce ab initio phonon spectra of nanostructures. *Computer Physics Communications* **2016,** *200*, 27-36.